

Static design of a liquid-salt-cooled pebble bed reactor (LSPBR)

S.J. de Zwaan, B. Boer, D. Lathouwers, J.L. Kloosterman *

Delft University of Technology (TUD), Mekelweg 15, 2629 JB Delft, The Netherlands

Received 3 July 2006; accepted 14 November 2006

Available online 22 January 2007

Abstract

A renewed interest has been raised for liquid-salt-cooled nuclear reactors. The excellent heat transfer properties of liquid-salt coolants provide several benefits, like lower fuel temperatures, higher average coolant temperature, increased core power density and better decay heat removal, and thus higher achievable core power. In order to benefit from the on-line refueling capability of a pebble bed reactor, the liquid salt pebble bed reactor (LSPBR) is proposed. This is a high temperature pebble bed reactor with a fuel design similar to existing HTRs, but using a liquid-salt as coolant. In this paper, the selection criteria for the liquid-salt coolant are described. Based on its neutronic properties, LiF–BeF₂ (flibe) was selected for the LSPBR. Two designs of the LSPBR were considered: a cylindrical core and an annular core with a graphite inner reflector. Coupled neutronic thermal-hydraulic calculations were performed to obtain the steady state power distribution and the corresponding fuel temperature distribution. Calculations were performed to investigate the decay heat removal capability in a protected loss-of-forced cooling accident. The maximum allowable power that can be produced with the LSPBR is hereby determined. © 2006 Elsevier Ltd. All rights reserved.

1. Introduction

Because of its high efficiency and inherent safety features, the high temperature gas-cooled reactor (HTGR) attracts a lot of attention worldwide. Despite these promising features, the HTGR concept can be improved by using a liquid-salt as a coolant instead of helium. Promising liquid-salt candidates exist that have excellent heat capacity and heat transfer properties, which allow reactor operation at high power density and high total power without any compromise to safety.

Till now, the Oak Ridge National Laboratory (ORNL) has focused on the advanced high temperature reactor (AHTR) (Forsberg et al., 2004), which can be considered as the liquid-salt-cooled counterpart of the prismatic HTGR. In this paper, we focus on the liquid-salt-cooled pebble bed reactor (LSPBR), which combines the advantages of a pebble-bed HTGR design (e.g. on-line refueling and flexible fuel management) with those of the AHTR

(e.g. reactor operation at ambient pressure, high power density, lower maximum fuel temperatures, etc.).

The LSPBR has a core volume of approximately 300 m³ and a core height of 7.5 m. It produces 2500 MWth heat at 1000 °C liquid-salt coolant outlet temperature. Both a cylindrical and an annular core are investigated. The fuel of the LSPBR consists of TRISO coated particles incorporated in regular HTR fuel pebbles. The TRISO particles consists of an UO₂ fuel kernel covered by a porous buffer layer and a combination of an inner pyrolytic carbon (IPyC), a silicon carbide (SiC) layer and an outer pyrolytic carbon layer (OPyC).

There is one major difference between the AHTR and the LSPBR. The first reactor design has some flexibility with regard to the salt volume fraction in the core, as this is a design parameter that can freely be chosen, while the LSPBR has a fixed salt volume fraction of about 39% determined by the porosity of the random packing of the pebble bed.

2. Selection of the liquid-salt coolant

Several criteria are important for the selection of a liquid-salt coolant. Apart from good heat transfer

* Corresponding author. Tel.: +31 15 27 81191; fax: +31 15 27 86422.
E-mail address: J.L.Kloosterman@tudelft.nl (J.L. Kloosterman).

coefficients, a coolant must be chemically inert, have low toxicity, reasonably low melting point and high boiling temperature. Furthermore, it must be compatible with the moderator and with common structural materials. Table 1 lists some important physical properties of the seven salt mixtures initially selected as candidates for the LSPBR (Forsberg et al., 2005; Zwaan, 2005).

All coolants moderate and absorb neutrons. When voiding occurs, the reactivity will increase due to the reduced absorption and decrease due to the reduced moderation. For a safe operation of the reactor it is required that the liquid-salt coolant does not lead to a positive voiding or temperature reactivity effect. This can be prevented by using a coolant with good moderating properties, which can be quantified by the moderating ratio. For all liquid-salt mixtures considered, the moderating ratio is shown in Table 1. The Σ_a and the Σ_s were calculated by flux weighting in the 0–1 eV and the 1–10⁴ eV regions, respectively, and ξ is the lethargy gain per collision (Duderstadt and Hamilton, 1976). Clearly, LiF–BeF₂ (flibe) has the best moderating ratio of all salts considered. Note that the lithium used in all salts is assumed to be highly enriched in ⁷Li to reduce neutron absorption. In flibe, the absorbing nuclide ⁶Li is produced via the ⁹Be(n, α) reaction and removed via neutron capture. This results in an equilibrium concentration of about 0.0007% (Forsberg et al., 2005; Zwaan, 2005).

In the remainder of this chapter, results are shown from calculations done with the SCALE (SCALE, 2005) code system using data based on JEF2.2. In all calculations a macro cell was modeled containing a smeared fuel region, a graphite layer and a coolant region. Because the SCALE code system cannot handle explicitly the double heterogeneity of the fuel, the cell-weighting procedure was split up in parts. First, a micro-cell calculation was done for TRISO coated particles, using BONAMI and NITAWL-II for the resonance shielding and XSDRNPM to generate a cross-section library for the homogenized fuel zone of the pebble. The outer radii of the kernel, buffer, and the IPyC, SiC, and OPyC layers in the TRISO particles were 0.025, 0.034, 0.038, 0.042 and 0.045 cm, respectively. The Dancoff factor used in the resonance shielding calculations was obtained by an analytical procedure (Bende et al., 1999) and takes into account the double heterogeneity of the fuel and the salt between the pebbles. In the second part, cross-sections for the 0.5-cm thick graphite layer surrounding the fuel zone, and the liquid salt coolant region were processed. Finally, all (three) libraries were merged and XSDRNPM was used to perform the cell weighing of the pebble and the calculation of the k_∞ .

2.1. Effect of fuel loading on the k_∞

For the seven candidate salts and for helium, the k_∞ is shown in Fig. 1 as a function of the inverse fuel loading. Clearly, for salts LiF–NaF–KF, NaF–ZrF₄–KF, and

Table 1
Physical properties and moderating ratio of the seven candidates salts (Forsberg et al., 2005; Zwaan, 2005)

Salt (mol %)	Molar mass (g/mol)	Melting point (°C)	Density (g/cm ³), T (°C)	700 °C Heat capacity (kJ kg ⁻¹ K ⁻¹)	Viscosity (mPa s), T (K)	Moderating ratio $\xi\Sigma_s/\Sigma_a$
⁷ LiF–BeF ₂ (66–34)	33.1	458	2.28–4.9 × 10 ⁻⁴ T	2.38	0.116 exp(3755/T)	63.0
NaF–BeF ₂ (57–43)	44.1	360	2.27–3.7 × 10 ⁻⁴ T	2.18	0.034 exp(5164/T)	9.8
⁷ LiF–NaF–KF (46.5–11.5–42)	41.2	454	2.53–7.3 × 10 ⁻⁴ T	1.88	0.04 exp(4170/T)	1.7
NaF–ZrF ₄ (50–50)	104.6	510	3.79–9.3 × 10 ⁻⁴ T	1.17	0.071 exp(4168/T)	6.7
NaF–ZrF ₄ –KF (10–48–42)	102.3	385	3.45–8.9 × 10 ⁻⁴ T (est.)	1.09 (est.)	0.061 exp(3171/T) (est.)	2.9
⁷ LiF–NaF–ZrF ₄ (42–29–29)	71.56	460	3.37–8.3 × 10 ⁻⁴ T	1.47	0.0585 exp(4647/T)	12.5
NaF–Na ¹¹ BF ₄ (8–92)	104.4	385	2.25–7.1 × 10 ⁻⁴ T	1.51	0.0877 exp(2240/T)	12.9

NaF–NaBF₄ the resulting k_{∞} is much too low. From the salts shown in Fig. 1, the curves of flibe resemble most those of helium. For all other salts, the curves bend downwards with decreasing fuel loading, indicating that neutron absorption in the salt increases.

2.2. Effect of voiding, temperature and packing fraction on k_{∞}

As in the previous section, the effects of the coolants on the neutronics were also studied in an infinite array of peb-

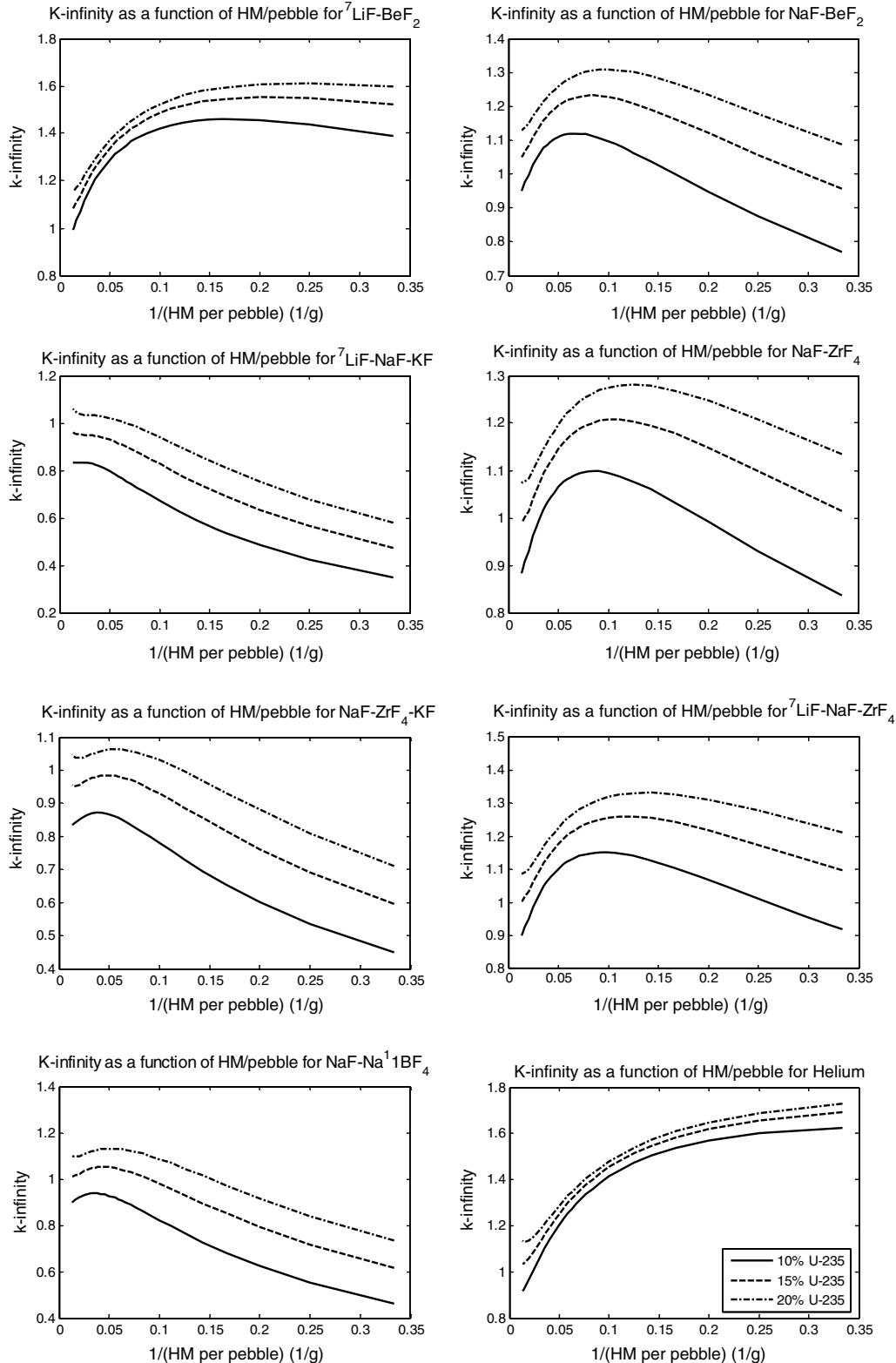


Fig. 1. The k_{∞} as a function of the inverse fuel loading for the seven candidate salts and for helium with the fuel enrichment as a parameter.

bles. In Table 2 the results of k_∞ calculations are given for the salts and for helium. The fuel loading per pebble was 12 g of uranium with a fuel enrichment of 10%. As can be seen, for three salts, the k_∞ is below unity. The first salt (flibe) gives a k_∞ comparable with that of the helium case.

It can be seen that for all salts except for flibe, complete voiding introduces a large positive reactivity (third column). If a loss of coolant accident (LOCA) occurs, the reactivity increase would have to be compensated by the fuel temperature reactivity coefficient. Fortunately, this coefficient is strongly negative in the absence of salt (see the results for helium coolant).

Several mechanisms like seismic shaking, loss of coolant flow and coolant temperature change (since the densities of some salts are close to that of the graphite pebbles) can alter the pebble bed porosity. Therefore, in Table 2, the porosity reactivity coefficient is shown in the fifth column. These values were obtained by increasing the bed porosity in the calculations with 1%. Since in the LSPBR both a decrease and an increase in porosity can occur, depending on the design and incident considered, any change in porosity should not lead to large reactivity effects. Among all liquid-salt candidates, flibe has the smallest porosity reactivity coefficient. The porosity reactivity coefficient for flibe is positive only for a limited range of the fuel loading, as can be seen in Fig. 2.

All properties in Table 2 depend on the fuel loading per pebble. In Fig. 3 the k_∞ is shown as a function of the inverse fuel loading per pebble. During burnup the fuel loading per pebble decreases (inverse loading increases) and the void reactivity coefficient is expected to become less negative or even positive. One has to note that in practice the core will be composed of pebbles with a wide range of burnup levels, and some average effective enrichment. No detailed burnup analysis has yet been performed. For flibe (left plot) with a fuel loading less than ~ 8.5 g (more than ~ 0.11 to 0.12 g⁻¹) per pebble, voiding leads to an increase in k_∞ . For all other salts, this is the case at all fuel loadings like in the right plot of Fig. 3.

Fig. 4 shows the combined temperature effects of the fuel and the coolant. For flibe, the sum of the fuel and coolant temperature reactivity coefficients remains negative until a fuel loading of ~ 3.9 g HM/pebble (0.26 g⁻¹). Three regions can be identified: In region I the Doppler reactivity

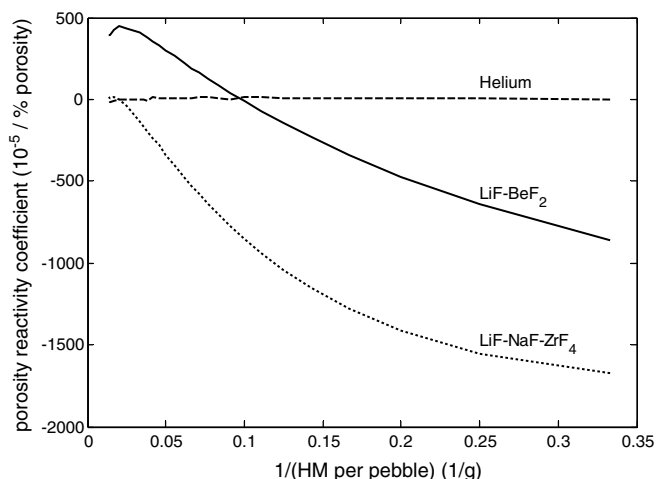


Fig. 2. The porosity reactivity coefficient for flibe and LiF–NaF–ZrF₄ as a function of the inverse fuel loading compared with that of helium.

coefficient and the coolant temperature feedback reinforce each other, in region II the coolant temperature coefficient is positive but the Doppler effect is negative and dominant, while in region III the positive coolant temperature coefficient has become dominant.

From all data shown above, it is clear that flibe seems the best candidate for application in the LSPBR. It has the best moderating quality; it gives the highest k_∞ values and strongly negative temperature reactivity coefficients. A disadvantage of flibe is that it consists of lithium enriched of the ⁷Li isotope, which will require expensive isotope separation. To avoid isotopic separation of a salt component, NaF–ZrF₄, NaF–BeF₂ or other salts not investigated in this study could be used. These options are less attractive with regard to parasitic neutron absorption and a large voiding reactivity coefficient. Because flibe has the best neutronic properties of all candidate salts, it was selected as the primary coolant for the LSPBR.

3. Parameter design for the LSPBR

As mentioned before, the major difference between the AHTR (Forsberg et al., 2004) and the LSPBR is the salt volume fraction in the core. The pressure drop over the packed pebble bed can be calculated with the Ergun relation (Beek et al., 1999):

Table 2
Some important reactivity coefficients for pebbles containing 12 g of uranium with fuel enrichment of 10%

Salt	k_∞	Reactivity change complete voiding (\$)	Uniform temperature reactivity coefficient ($10^{-5}/K$)	Porosity reactivity coefficient ($10^{-5}/\%$ porosity)
⁷ LiF–BeF ₂	1.39	–2.30	–7.68	+70
NaF–BeF ₂	1.11	21.5	–2.53	–860
⁷ LiF–NaF–KF	0.71	87.9	8.14	–1290
NaF–ZrF ₂	1.10	23.0	–0.47	–870
NaF–KF–ZrF ₄	0.81	65.1	5.42	–1310
⁷ LiF–NaF–ZrF ₄	1.15	17.7	–1.53	–730
NaF–Na ¹¹ BF ₄	0.86	56.2	8.32	–1250
Helium	1.36	–0.11	–8.58	+30

All coolants are at ambient pressure except for helium which is assumed to be at 7 MPa.

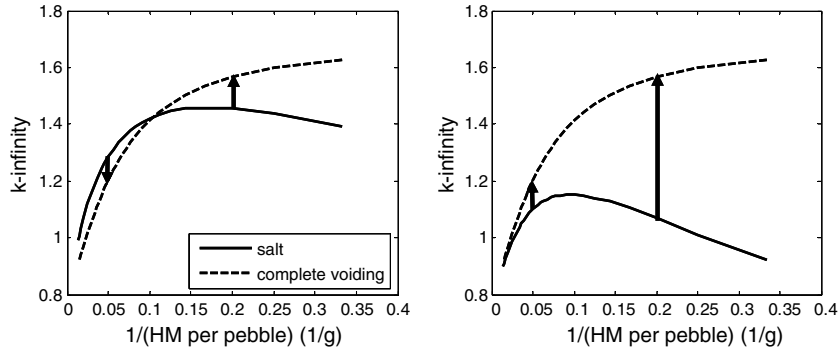


Fig. 3. The k_{∞} as a function of the fuel loading per pebble for flibe (left) and LiF–NaF–ZrF₄ (right), both combined with the complete voided case. In a LOCA, the k_{∞} of the liquid salt moves to that of the complete voiding case.

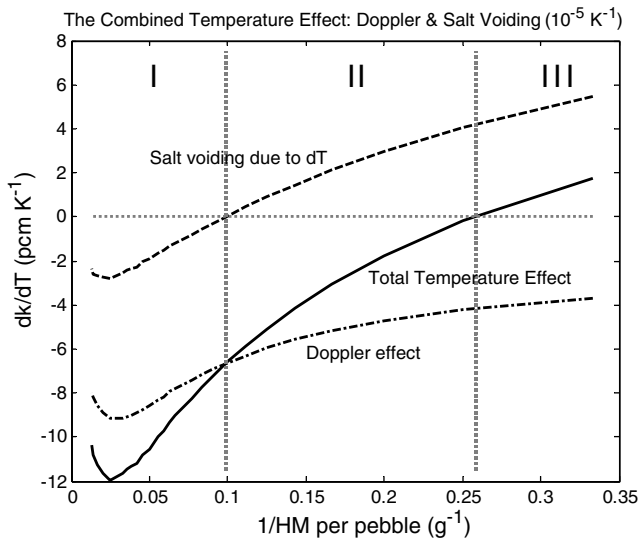


Fig. 4. The combined temperature effect, the change in k_{∞} per kelvin is shown as a function of salt voiding, the Doppler effect and the combined temperature reactivity coefficient.

$$\Delta p = \frac{1 - \varepsilon}{\varepsilon^3} \left(170 \frac{\mu}{\rho v_0 d_p} (1 - \varepsilon) + 1.75 \right) \frac{H}{d_p} \rho v_0^2 \quad (1)$$

Here ε is the porosity of the pebble bed (or the coolant volume fraction), μ the dynamic viscosity, ρ the density of the coolant, v_0 the superficial coolant velocity through the core, d_p the pebble diameter and H the height of the reactor core. Using

$$v_0 = \frac{\dot{m}}{\rho A} \quad (2)$$

where \dot{m} is the coolant mass flow rate and A is the cross-sectional area of the reactor, this equation can be rewritten as

$$\Delta p = \frac{1 - \varepsilon}{\varepsilon^3} \left(170 \frac{\mu A}{\dot{m} d_p} (1 - \varepsilon) + 1.75 \right) \frac{H}{d_p \rho} \left(\frac{\dot{m}}{A} \right)^2 \quad (3)$$

The mass flow of the coolant inside the reactor core can be calculated with the relation

$$\dot{m} = \frac{P}{c_p \Delta T} \quad (4)$$

Here c_p is the heat capacity of the coolant, P the total thermal power of the reactor and ΔT the temperature difference of the coolant between the inlet and outlet of the core.

Two different core shapes, both with a height of 750 cm, have been investigated: an annular core with an outer radius of 100 cm and an inner reflector with radius of 360 cm, and a cylindrical core with an outer radius of 360 cm. The core volume in both cases equals about 300 m³, and the average power density 8.3 MW/m³. The total power thus equals 2500 MWth in both cases. In this design the pebble bed is pressed together to a packed bed by the coolant flow from top to bottom. The salt enters the core at the top of the core at a temperature of 900 °C and will be heated up to 1000 °C at the bottom of the core. To achieve this, the mass flow rate is set to 10,478 kg/s. In the annular core, the heated salt returns to the top through the inner reflector, which enables one to use a reactor vessel with no exit at the bottom. In Table 3, the data needed to calculate the pressure drop are shown, as well as the resultant pressure drop, which is less than one bar.

For both the annular core and the cylindrical core shape, the same pebbles were used as a fuel. The inner zone of each pebble fueled with TRISO particles had a radius of 2.5 cm, while the outer radius of the graphite layer was 3 cm. The density of the graphite was 1.7 g cm⁻³ and contained 0.75 ppm natural boron as an impurity. The total fuel loading per pebble was 8 g of uranium 10% enriched

Table 3

Results of the pressure drop calculations for flibe in a reactor core with height of 7.5 m and volume of 300 m³

Parameter (flibe)	Value
Density ρ at 950 °C (kg m ⁻³)	1815.7
Dynamic viscosity μ at 950 °C (mPa s)	2.50×10^{-3}
Heat capacity c_p (kJ kg ⁻¹ K ⁻¹)	2.38
Mass flow (kg s ⁻¹)	10478
Average coolant velocity (m s ⁻¹)	0.36
Reynolds number	6300
Pressure drop (MPa)	0.078
Pumping power (kW)	451
Fraction of total electric power of 1300 MW (%)	0.032

The total thermal power is 2500 MW and the salt is assumed to be heated from 900 °C at the inlet (top) to 1000 °C at the outlet (bottom).

Table 4
Dimensions of the two core geometries

Parameter	Cylindrical core	Annular core
Core height (m)	7.5	7.5
Core outer diameter (m)	3.60	3.70
Inner reflector radius (m)	n. a.	1.0
Core volume (m ³)	305.36	299.0
Volume fraction fuel zone (TRISO particles and graphite)	0.35	0.35
Vessel diameter (m)	9.00	9.20
Vessel height (m)	16.60	16.60
Vessel thickness (m)	0.10	0.10
Argon gap (m)	0.10	0.10
Guard vessel thickness (m)	0.02	0.02
Outer reflector thickness (m)	0.80	0.80
Top reflector thickness (m)	2.00	2.00
Top reflector thickness (m)	1.50	1.50
Porosity top and bottom reflector (fraction of solid material)	0.50	0.50
Porosity top and bottom plenum (fraction of solid material)	0.1	0.1
Top plenum inner/outer diameter/height (m)	0.0/3.6/2.0	1.0/3.7/2.0
Bottom plenum inner/outer diameter/height (m)	0.0/3.6/2.0	0.0/3.7/2.0

in ²³⁵U. In Table 4, the dimensions of the two core geometries are given.

4. Steady state operation

To examine the behavior of the LSPBR during normal operation, steady state calculations were performed with a coupled neutronics and thermo-hydraulics code system. For the first the 3-D neutron transport code EVENT (de Oliveira, 1986) was used, while for the latter a modified version of the well-known THERMIX code (Struth, 1995) was used. Two-group temperature-dependent cross sections were generated with the SCALE code system (SCALE, 2005). The steady state solution of a core configuration is found by iteratively transferring the power distribution from EVENT to THERMIX and returning the temperature distribution to EVENT. An additional poison was homogeneously mixed with the fuel to reach a k_{eff} of 1 at a power level of 2500 MWth. More details about this coupling scheme can be found in Zwaan (2005).

Table 5
Results of steady state calculations for the annular and the cylindrical core

Parameter	Cylindrical core	Annular core
Power level (MWth)	2500	2500
Average power density \bar{P} (MWth/m ³)	8.19	8.36
Maximum power density P_{max} (MWth/m ³)	16.8	14.7
Peak factor (P_{max}/\bar{P})	2.05	1.75
Average velocity of salt in the pebble bed (m/s)	0.36	0.37
Coolant inlet temperature (°C)	900	900
Coolant outlet temperature (°C)	1000	1000
Maximum coolant temperature (°C)	1051	1028
Maximum fuel (pebble centre) temperature (°C)	1190	1152

In Table 5 the steady state results are summarized, while Fig. 5 shows the steady state power density profiles in the two core geometries. The main advantage of the annular core seems the lower peaking factor and the corresponding lower maximum power density.

In Fig. 6, we show the maximum fuel temperature profile (at the center of the pebbles) and the maximum coolant temperature in the LSPBR. The maximum fuel temperature is around 1190 °C for the cylindrical core and 1150 °C for the annular. These values compare quite well with the AHTR, in which the maximum fuel temperature is around 1180 °C (Forsberg et al., 2004). Due to the lower power peaking in the annular core the ratio of the maximum fuel temperature and maximum coolant temperature is more favorable as well.

As mentioned above, the steady state power profile was found by adding a poison to the fuel to reach a k_{eff} of 1 at a power of 2500 MWth. In reality, the core will continuously be refueled. Fresh fuel is added at the top of the core, while (partially) burned fuel is unloaded at the bottom. This will move the maximum in the power profile towards the top of the core (the cooler region) and therefore also the maximum temperature difference between the fuel and coolant. This will probably lead to lower values of the maximum fuel temperature.

5. Passive decay heat removal

In a loss-of-forced cooling incident (LOFC), the fission product decay heat cannot be removed by the coolant and the secondary cooling system. Instead it should be removed from the core by natural convection of the salt, convective heat transfer from the coolant to the reflector, conduction in the reflector and thermal radiation as shown in Fig. 7. The maximum power that can be produced in the LSPBR is limited by the temperatures that are reached during a LOFC.

Although THERMIX is a standard code to handle thermal hydraulics calculations of gas-cooled pebble bed reactors, it is not suitable for decay heat removal calculations in the LSPBR. In THERMIX the interaction between the solid material and the fluent coolant is programmed between two numeric fields, the convection field and the solid material field, as shown in Fig. 8. Heat can be transferred from the center mesh of the core to the outside mesh

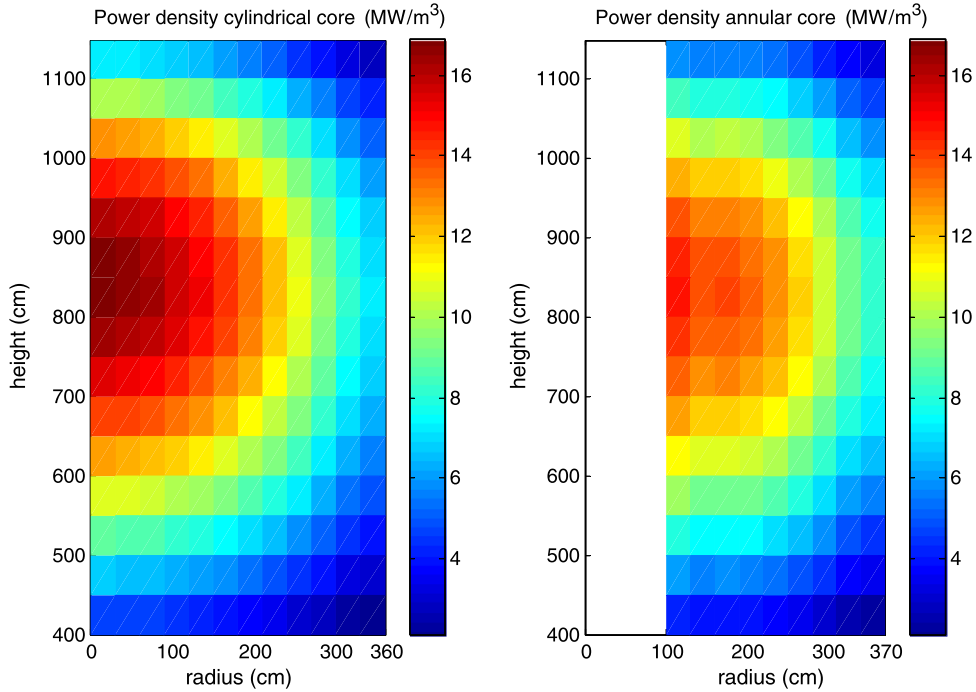


Fig. 5. Power density in the cylindrical core (left) and the annular core (right).

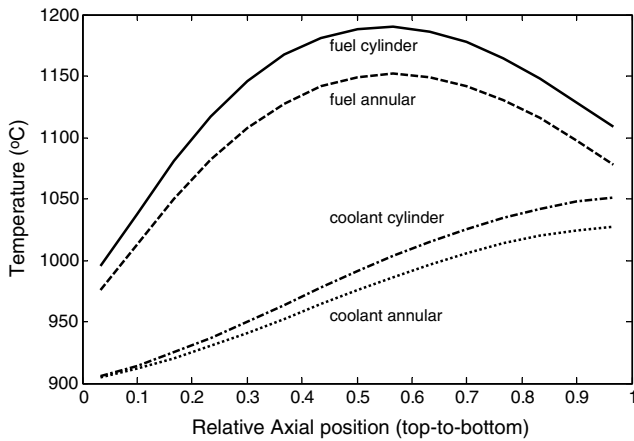


Fig. 6. The axial profiles of the maximum fuel temperatures and the maximum coolant temperature of the 2500 MWth LSPBR (annular and cylindrical). Due to the higher power peaking factor in the cylindrical core, the maximum fuel temperature and coolant exit temperature are higher.

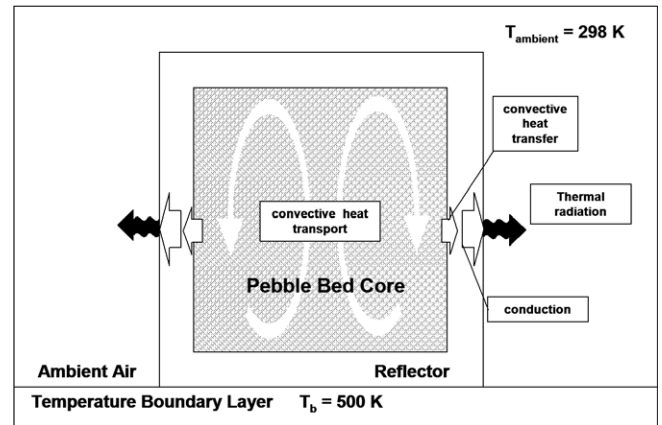


Fig. 7. Decay heat removal mechanisms in the LSPBR. The decay heat is removed from the core by natural convection, convective heat transfer from the coolant to the reflector, conduction in the reflector and thermal radiation from the core vessel to the ambient air with a temperature of 298 K. The bottom boundary condition was set at 500 K.

of the core by (natural) convection but from there it must be transferred out of the core by conduction (in the solid material calculation). In the LSPBR, the convective heat transfer from the coolant to the reflector is the main heat transport mechanism in decay heat removal problems. Therefore, to examine the temperature distribution during a LOFC with scram, the decay heat calculations were performed with the code HEAT (Lathouwers and Bellan, 2001).

The code HEAT can solve time-dependent natural circulation problems in packed beds and was originally written for fluidized beds in chemical applications (Lathouwers and Bellan, 2001), but has been modified for several other

applications, like the decay heat removal in the fluidized bed nuclear reactor (Agung et al., 2006). The code HEAT has the benefit that the convective coolant field is connected to the solid reflector field (as shown in Fig. 8) so that convective heat transfer between the coolant and the reflector is taken into account. The solid conduction heat transfer between the pebble bed and the reflector is neglected in this code.

In this paper, the analysis is limited to the cylindrical core geometry with graphite reflectors, which is considered the least favorable geometry for decay heat removal.

The fission product decay power can be written as a fraction of the initial prompt power P_p :

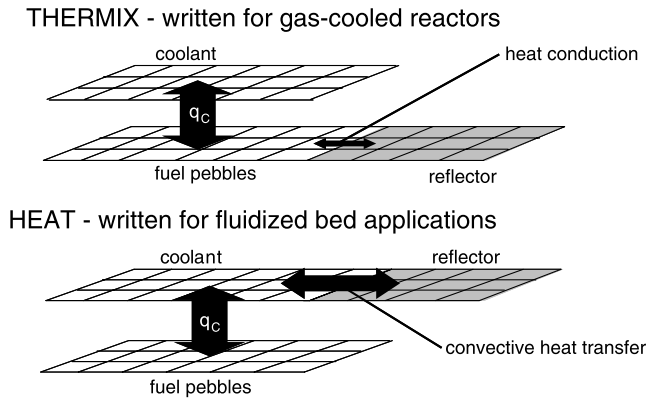


Fig. 8. The difference between the thermal hydraulics code THERMIX and HEAT. In both codes there is interaction between the convection grid and the solid grid through heat sources and sinks in the core. In THERMIX the heat transfer to the reflector is modeled by conduction from the core to the reflector, while in HEAT the heat is transported from the coolant to the reflector by convective heat transfer.

$$P_{d,n} = \sum_{n=1}^{N_d} \frac{\gamma_n P_p}{Q_f \lambda_n} e^{-\lambda_n t} \quad (5)$$

Here $P_{d,n}$ is the decay power of group n , Q_f is the prompt energy per fission and γ_n is the decay heat yield. This expression can be written as a function of the total power as

$$P_{d,n} = \frac{P_{\text{tot}}}{Q_f + \sum_{n=1}^{N_d} \frac{\gamma_n}{\lambda_n}} \sum_{n=1}^{N_d} \frac{\gamma_n}{\lambda_n} e^{-\lambda_n t} \quad (6)$$

This relation is applied in HEAT to calculate the fission product decay power using data for 23 groups from (DIN, 1990). The code uses an analytical expression for the power profile given as a zero order Bessel function in radial direction and a sine function in axial direction (Duderstadt and Hamilton, 1976). A set of balance equations for momentum and energy is discretized and solved using the finite volume method with a staggered grid. Time discretization is based on backward Euler scheme in combination with a pressure correction technique. The theory used in HEAT is described in more detail in Zwaan (2005).

Two cases were investigated. The first is a pebble bed with coolant surrounded by a graphite reflector, while the second has an additional 7.5 m high salt plenum on top of the pebble bed. Various initial power levels were used in the simulations to determine the maximum power possi-

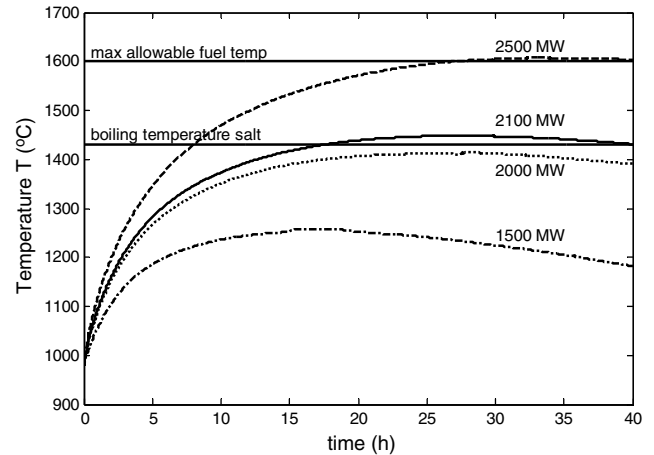


Fig. 9. The maximum fuel temperature as a function of time with the initial power as a parameter; geometry without salt plenum.

ble without exceeding the limits on fuel temperature and coolant temperature. All simulations were run for 40 h of real time.

In Fig. 9, we show the maximum fuel temperature as a function of time with the initial power level as a parameter. The thermal transients show an increase in core temperature during the first few hours after which the core gradually cools down. Note that the maximum coolant temperature does not differ much from the maximum fuel temperature shown in the figure. At first the heat transfer from the coolant to the reflector is insufficient to compensate for the decay power produced inside the core. The salt and core are heated and a natural convection flow is induced inside the core. Because of the thermal inertia of the salt the heating of the core will take several hours. When the coolant flow induced by natural convection increases, the convective heat transfer to the reflector wall increases until it exceeds the decay heat power produced in the fuel. Then, the coolant and the fuel will gradually cool.

There are two temperature limits that need to be considered: the maximum of 1600 °C for TRISO coated fuel particles and the temperature at which the salt coolant starts to boil (1430 °C). Because the latter phenomenon could not be modeled in HEAT, the lowest temperature limit is chosen to be restrictive. This means that for the geometry *without* a salt plenum on top of the core, the maximum power is 2000 MWth. In Table 6, the resultant maximum

Table 6

Maximum fuel and coolant temperatures and times in the transient at which these temperatures are reached for the geometry *without* additional salt plenum

Initial power (MW)	Max fuel temperature (°C)	Time at max temperature (h)	Max coolant temperature (°C)	Time at max temperature (h)
500	1023	4.5	1023	4.5
1000	1116	8.6	1116	8.6
1500	1257	16.1	1253	17.3
2000	1415	27.8	1412	24.8
2100	1448	26.0	1447	26.0
2500	1607	33.3	1606	33.1

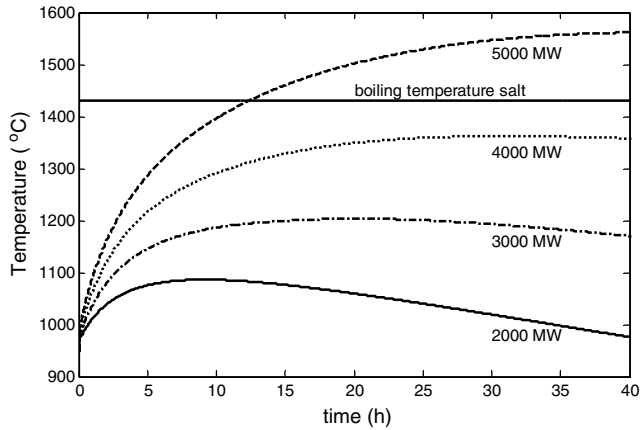


Fig. 10. The maximum fuel temperature as a function of time with the initial power as a parameter; geometry includes a salt plenum on top of the core.

temperatures reached in the transient are given, as well as the times at which these are reached.

For the geometry with a 7.5 m high additional salt plenum on top of the core, the total volume of salt is larger by a factor of 3.5. So much more decay heat can be stored without exceeding the limits on the coolant and fuel temperatures. Furthermore, the outer surface of the reactor core is enlarged with a factor of 1.7, which enhances considerably the heat transfer from the salt to the graphite reflector. In Fig. 10 the maximum fuel temperature is shown as a function of time with the initial power as a parameter ranging from 2000 to 5000 MWth.

Only in the 5000 MWth case the maximum fuel temperature exceeds the boiling temperature of flibe (1430 °C). The highest permissible power in the LSPBR with a 7.5 m high salt plenum is about 4000 MWth. This result is comparable to that of the University of California at Berkeley for a 4000 MWth core, which yielded a peak core temperature of 1325 °C as reported in (Forsberg et al., 2004). In Table 7, the maximum temperatures during the transient are shown together with the times at which these are reached.

In Fig. 11, we show the maximum fuel temperature as a function of time for the cylindrical geometry with and without a salt plenum. Without a salt plenum, the fuel reaches a temperature of 1415 °C at an initial power level of 2000 MWth. When the 7.5 m high salt plenum is present,

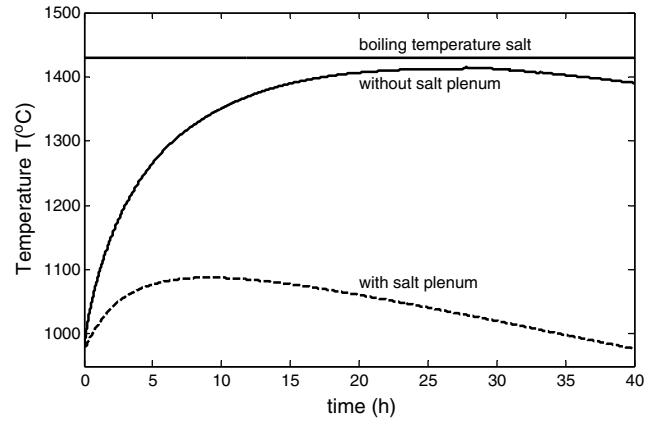


Fig. 11. Maximum fuel temperature as a function of time after a LOFC incident for the cylindrical cores with and without a salt plenum. In both cases the reactor power is 2000 MWth.

the maximum temperature of the fuel remains below 1090 °C for the same initial power level, which clearly shows the effect of the introduced additional thermal inertia of the salt in the plenum.

The time at which the fuel temperature reaches its maximum is also different. Without plenum the maximum temperature is reached after 27.8 h while with plenum this is reached already after 9.1 h. This means that not only the capability to absorb energy is increased; also the capability to transfer heat from the core to the graphite reflector is increased. Not only the total surface through which the heat can be transferred is much larger with an additional salt plenum, there is also more salt available to store and remove the heat from the core.

6. Conclusions

From the seven liquid-salt candidates considered in this paper, the best choice for the LSPBR is LiF–BeF₂ (flibe). It has the highest moderating ratio; it gives the highest k_{∞} value, a small porosity reactivity coefficient, a negative coolant voiding reactivity coefficient and the strongest negative temperature reactivity coefficient.

An investigation of the core dimensions of the LSPBR was made. The height of the pebble bed core is not restricted by the pressure drop. For a core height of 7.5 m and a volume of 300 m³ the pressure drop will be less than 1 bar.

Table 7

Maximum fuel and coolant temperatures and times in the transient at which these are reached for the geometry including a salt plenum

Initial power (MW)	Max fuel temperature (°C)	Time at max temperature (h)	Max coolant temperature (°C)	Time at maximum temperature (h)
2000	1087.7	9.1	1086.4	8.9
2100	1097.5	9.6	1096.2	9.6
2500	1193.3	13.4	1137.9	13.5
3000	1205.0	19.4	1203.6	20.0
4000	1364.2	30.0	1362.5	30.4
5000	Not reached		Not reached	

As can be expected, it is found that the power density is largest in the center of the core. Because of the lower fuel temperatures in the annular geometry, this is the preferred core shape for the liquid-salt pebble bed reactor. Compared to the AHTR the annular LSPBR has lower maximum fuel temperatures.

An investigation was made of the decay heat removal capability of the cylindrical reactor core by passive means. The maximum allowable nominal power is 2000 MWth without salt plenum and 4000 MWth with a 7.5 m high salt plenum on top of the core. Then the boiling temperature of flibe (1430 °C) is not exceeded.

Future work on this reactor concept will consist of a depletion analysis of the fuel to determine the maximum fuel burnup that can be achieved with the LSPBR. Also several accident scenarios and transients will be investigated.

Acknowledgements

The authors thank the Oak Ridge National Laboratory and Dr. C.W. Forsberg for their support on this project and for the information provided on the AHTR project.

References

- Agung, A., Lathouwers, D., Hagen, T.H.J.J., van der, Dam, H. van, Pain, C.C., Goddard, A.J.H., Eaton, M.D., Gomes, J.L.M.A., Miles, B., de Oliveira, C.R.E., 2006. On an improved design of a fluidized bed nuclear reactor. I. Design modifications and steady-state features. *Nucl. Sci. Eng.* 153, 117–131.
- Beek, W.J., Mutzall, K.M.K., Heuven, J.W. van, 1999. *Transport Phenomena*. John Wiley and Sons, London 0-471-99977-6.
- Bende, E.E., Hogenbirk, A.H., Kloosterman, J.L., Dam, H. van, 1999. Analytical calculation of the average Dancoff factor for a fuel kernel in a pebble bed high-temperature reactor. *Nucl. Sci. Eng.* 133, 147–162.
- DIN, 1990. Berechnung der Nachzerfallsleitung der Kernbrennstoffe von Hochtemperatur reactoren mit kugelförmigen Brennelementen, Technical Report DIN 25 485, Deutsches Institut für Normung e.v.
- Duderstadt, J.J., Hamilton, L.J., 1976. *Nuclear Reactor Analysis*. John Wiley and Sons, New York, ISBN 0-471-22363-8.
- Forsberg, C.W., Peterson, P.F., Pickard, P.S., 2004. Status of the preconceptual design of the advanced high-temperature reactor, (AHTR) ORNL/TM-2004/104. Oak Ridge national Laboratory, Oak Ridge, USA.
- Forsberg, C.W., Peterson, P.F., Williams, D.F., 2005. Liquid-salt cooling for advanced high-temperature Reactors. In: *Proceedings of the ICAPP'05*, Seoul, Korea.
- Lathouwers, D., Bellan, J., 2001. Modeling of dense gas-solid reactive mixtures applied to biomass pyrolysis in a fluidized bed. *Int. J. Multiphase Flow* 27, 2155.
- Oliveira, C.R.E., 1986. An arbitrary geometry finite element method for multigroup neutron transport with anisotropic scattering. *Prog. Nucl. Energy*, 227–236.
- SCALE, 2005. SCALE: A Modular Code System for Performing Standardized Computer Analyses for Licensing Evaluations, vols I–III. ORNL/TM-2005/39, version 5, Oak Ridge National Laboratory.
- Struth, S., 1995. THERMIX-DIREKT, Ein Rechenprogramm zur Instationearen, Zweidimensionalen Simulation Thermohydraulischer Transienten. Forschungszentrum Jülich, Jülich, Germany.
- Zwaan, S.J. de, 2005. The liquid salt pebble bed reactor, a new high temperature nuclear reactor, MSc thesis, Delft University of Technology. Online available at www.rrr.tudelft.nl/pnr (select “publications” and “master theses”).